PERGAMON

International Journal of Multiphase Flow 28 (2002) 225–246

International Journal of Multiphase Flow

www.elsevier.com/locate/ijmulflow

Experimental verification of the force coupling method for particulate flows

S. Lomholt [a], B. Stenum [a], M.R. Maxey [b,*]

[a] *Risø National Laboratory, Roskilde, Denmark*

[b] *Division of Applied Mathematics, Brown University, P.O. Box 1966, 37 Manning Street, Providence, RI 02912, USA*

Received 29 September 2000; received in revised form 29 April 2001

Abstract

A force coupling method for computing particulate flows is verified by comparison with experiments. The force coupling method and the experimental method are briefly described. In the comparison three examples are considered: a single particle rising in an inclined channel, two particles rising in a vertical channel and three particles rising in a vertical channel. It is shown that for the particle Reynolds numbers considered in this paper ($Re_p < 15$) the force coupling method provides qualitatively and quantitatively good results. Consequently, the method is an attractive alternative to direct methods for simulations of particulate flows.

Keywords: Two-phase flow; Experiment; Numerical simulation; Particle interaction

1. Introduction

Two-phase flows with particles dispersed in a liquid are commonly encountered in biological and chemical engineering as well as in the processing of materials. Important aspects of these flows are the coupling between the particle motion and the liquid flow and the hydrodynamic interaction between the particles or the particles and a boundary. These aspects are not included in any of the standard equations of motion for particles, Maxey and Riley (1983). One source for these effects is the nonlinearity of the inertia terms, which results in an asymmetric flow around the particle. Further, viscous Stokes flow can lead to long-range interactions between particles.

* Corresponding author. Tel.: +1-401-863-1482; fax: +1-401-863-2722.
E-mail address: maxey@cfm.brown.edu (M.R. Maxey).

0301-9322/02/$ - see front matter
PII: S0301-9322(01)00045-3

Although semi-empirical equations of motion for the particles valid at high Reynolds numbers exist, such as Lawrence and Mei (1995) and Kim et al. (1998), these are still limited to small particles. Furthermore, they do not include a method for calculating the coupling between the particles and the fluid flow or the hydrodynamic interaction between particles or the effect of a wall (Michaelides, 1997).

So, how is it possible to compute the particle motion in a flow with important fluid inertia and/or large particles, when the hydrodynamic force on the particles is unknown? The straightforward method is to do a direct numerical simulation, where the flow around the particles is fully resolved. The hydrodynamic force is found from the pressure and shear stress distribution on each of the particles and the particles are moved in correspondence with these forces. For example, in the present finite element methods this requires the generation of a new mesh at each timestep and if a particle is close to a wall or to another particle a very fine mesh is needed in order to resolve the flow within this region. Therefore direct simulations are computationally extremely expensive and the number of particles is limited. Nevertheless, they have been performed in both two and three dimensional flows by Feng et al. (1994), Hu (1996) and Johnson and Tezduyar (1997). Other simulation methods have been developed by Esmaeeli and Tryggvason (1998) and Glowinski et al. (1999) that use a fixed static grid, but again the need to fully resolve the flow around each particle means the calculations are still computationally intensive. These direct simulations however do provide important information about the hydrodynamic forces and the flow around the individual particles.

An alternative simulation approach is the approximate force coupling method. This method has recently been developed by Maxey et al. (1997), Maxey and Dent (1998), Dent (1999), Lomholt (2000) and Maxey and Patel (2001). The force coupling method has several advantages in comparison with the direct numerical simulations. Firstly, the same mesh is used throughout the simulation. Therefore no time is used on remeshing, resulting in a much faster computation. Secondly, the method is relatively easy to implement in already existing codes for solving the Navier–Stokes equations. Finally, the approximate method can be used with a much lower level of resolution by contrast to the direct simulations, allowing a greater range of length scales in the flow to be simulated. The disadvantage of the force coupling method is that the hydrodynamic forces on the particles are not known to the same degree of accuracy as in the direct numerical simulations.

In this paper we report on a series of experiments on buoyant, spherical particles moving under gravity in a three-dimensional channel and use these to provide a comparison with corresponding flow simulation results obtained using the force coupling method. The comparisons are for particle Reynolds number below $Re_p < 15$, based on the sphere diameter and the Stokes settling velocity. The aim of the paper is to verify the results from the force coupling model and illustrate the applicability of the model. We will consider three cases: a single sphere, two spheres and three spheres rising in a vertical or inclined channel. Other experiments have been reported recently by Gondret et al. (1999) for a particle settling towards a single wall and by Wu and Manasseh (1998) for a pair of particles settling under gravity in a large tank, both for a similar range of Reynolds numbers. In the present simulations and experiments we are able to maintain a close match of the physical conditions. In the following sections we describe briefly the force coupling model and the numerical methods, the experimental procedures and then the results of the three different experiments.

2. The force coupling method

2.1. The force coupling model

Consider N equal rigid spherical particles with radius a and uniform density ρ_p dispersed in a domain surrounded by the surface S. The fluid is assumed to be an incompressible Newtonian liquid at a constant temperature. The particles exert a force and/or a torque on the fluid with an equal but opposite directed force and/or torque from the fluid on the particles. In the force coupling model the entire domain is considered as fluid, including the volume occupied by the particles. The force and torque from each of the particles on the fluid are represented by a force and torque distribution applied over a finite volume. The equations governing the fluid motion are

$$\frac{\partial u_i}{\partial x_i} = 0, \tag{1}$$

$$\rho_f\left(\frac{\partial u_i}{\partial t} + u_j\frac{\partial u_i}{\partial x_j}\right) = -\frac{\partial p}{\partial x_i} + \mu\frac{\partial^2 u_i}{\partial x_j \partial x_j} + \sum_{n=1}^{N}\left(F_i\Delta(\mathbf{x}-\mathbf{Y}^n,\sigma_m) + F_{ij}^n\frac{\partial\Delta(\mathbf{x}-\mathbf{Y}^n,\sigma_d)}{\partial x_j}\right), \tag{2}$$

where ρ_f, u_i, p and μ are the fluid density, velocity, pressure and dynamic viscosity, respectively. The center of mass of the nth particle is at Y_i^n and the force distribution is given by

$$\Delta(\boldsymbol{x}-\boldsymbol{Y}^n,\sigma) = \frac{1}{(2\pi\sigma^2)^{3/2}}\exp\left(-\frac{(x_i-Y_i^n)(x_i-Y_i^n)}{2\sigma^2}\right). \tag{3}$$

The width of the Gaussian, σ, is related to the particle radius, a and determines the distance from the particle center over which the force or torque acts. The first term in the summation is called a force monopole and the second term is called a force dipole.

The force from the nth particle on the fluid is given by the force monopole strength F_i. It consists of the body forces on the particle, i.e., the buoyancy force and the particle inertia. In this paper particle inertia is neglected. This means that particle accelerations in the flow are small compared to the gravitational acceleration g_i (Lomholt, 2000), i.e.,

$$\left|\frac{\mathrm{d}V_i}{\mathrm{d}t}\right| \ll |g_i|, \tag{4}$$

where V_i is the particle velocity. The force monopole strength, F_i, is therefore given as

$$F_i = (m_p - m_f)g_i = V_p(\rho_f - \rho_p)g_i, \tag{5}$$

where V_p is the volume of the particle and m_p and m_f are the mass of the particle and the displaced fluid, respectively.

The force dipole strength F_{ij}^n contains a symmetric and an antisymmetric part. The antisymmetric part is related to the torque from the particle on the fluid, while the symmetric part is related to the rate of strain field. In line with the neglect of the particle inertia and the time derivative of the particle velocity, we assume the time derivative of the particle angular velocity to be zero and neglect the inertia associated with the angular momentum of the particles. Therefore the

torque from the particle on the fluid is due to the external body torque on the particle. The antisymmetric tensor resulting from this is given by

$$T_{ij} = \frac{1}{2}\varepsilon_{ijk}T_k, \tag{6}$$

where T_i is the external body torque and ε_{ijk} is the alternating sign tensor (Lomholt, 2000). Since we consider spherical particles with a uniform density no external torque acts on the particles and the antisymmetric part of the F_{ij}^n is zero. The particles are considered as rigid spheres, therefore the rate of strain inside the volume occupied by the particles should be zero, at least in an average sense. The goal for the symmetric part of the force dipole strength is to adjust it in such a way, that the rate of strain averaged over a local volume is zero for the complete flow. The local volume averaged rate of strain is measured as

$$\tilde{E}_{ij} = \int E_{ij}\Delta(\mathbf{x} - \mathbf{Y}^{\mathbf{n}}, \sigma_{\mathrm{d}})\,\mathrm{d}^3\mathbf{x} \tag{7}$$

with the rate of strain tensor

$$E_{ij} = \frac{1}{2}\left(\frac{\partial u_i}{\partial x_j} + \frac{\partial u_j}{\partial x_i}\right). \tag{8}$$

In the standard multipole expansion for Stokes flow the symmetric part of F_{ij}^n is called the stresslet and for a fixed sphere in a pure straining Stokes flow the stresslet is (Kim and Karrila, 1991)

$$F_{ij} = \frac{20}{3}\pi\mu a^3 E_{ij}^{\infty}, \tag{9}$$

where E_{ij}^{∞} is the rate of strain of the undisturbed flow, u_i^{∞}. In the force coupling model the stresslet is similarly defined as

$$F_{ij} = \frac{20}{3}\pi\mu a^3 E_{ij}^{*}, \tag{10}$$

where E_{ij}^{*} is computed as the local volume average from the undisturbed flow, i.e.,

$$E_{ij}^{*} = \int E_{ij}^{\infty}\Delta(\mathbf{x} - \mathbf{Y}^{\mathbf{n}}, \sigma_{\mathrm{d}})\mathrm{d}^3\mathbf{x}. \tag{11}$$

For a fixed sphere in pure straining Stokes flow, computing F_{ij} using (10) and (11) and solving the momentum equation

$$-\frac{\partial p}{\partial x_i} + \mu\frac{\partial^2 u_i}{\partial x_j \partial x_j} = F_{ij}\frac{\partial\Delta(\boldsymbol{x}, \sigma_{\mathrm{d}})}{\partial x_j}, \tag{12}$$

results in a flow field that satisfies the condition of zero volume-averaged rate of strain (7) provided the ratio a/σ_{d} is appropriately set, Lomholt and Maxey (2001).

When the nonlinear inertia terms are included and the flow is time dependent, an a priori determination of the force coupling stresslet is not possible. Therefore the elements in F_{ij} must be computed iteratively. The elements are computed in the following manner:

1. Compute the velocity field with a force dipole strength

$F_{ij}^{[q-1]} = \frac{20}{3}\pi\mu a^3 E_{ij}^{*[q-1]}$.

If $q = 1$, then the final value of F_{ij} from the previous timestep is chosen.

2. From the new velocity field compute the volume average rate of strain using (7), i.e.,

$$\tilde{E}_{ij}^{[q-1]} = \int E_{ij}^{[q-1]} \Delta(\mathbf{x} - \mathbf{Y}, \sigma_\mathrm{d}) \mathrm{d}^3\mathbf{x}.$$

3. If $\tilde{E}_{ij}^{[q-1]} < \epsilon$, the computed velocity field is correct, proceed to the next timestep. Otherwise set $E_{ij}^{*[q]} = E_{ij}^{*[q-1]} + \tilde{E}_{ij}^{[q-1]}$.

4. Compute the new force dipole strength as

$F_{ij}^{[q]} = \frac{20}{3}\pi\mu a^3 E_{ij}^{*[q]}$

and return to 1.

The evaluation of the force coupling stresslet given in (10) is based on the definition from Stokes flow. This estimate is good for low Reynolds numbers and can also be used at higher Reynolds numbers. However, for finite Reynolds numbers it may not be the best estimate, thus a different definition could be better and this is a subject for future research. In this paper the definition given in (10) is used.

The above method provides the velocity field of the fluid including the effect of the particles. However, it does not provide the particle velocities directly. The particle velocities are determined as a local volume averaged velocity, $\tilde{u}_i$, in terms of the Gaussian envelope function

$$V_i^n(t) = \tilde{u}_i(t) = \int u_i(\mathbf{x}, t) \Delta(\mathbf{x} - \mathbf{Y^n}, \sigma_\mathrm{m}) \, \mathrm{d}^3\mathbf{x}, \tag{13}$$

where V_i^n is the velocity of the nth particle and the integration is over the entire computational domain. This is based on the idea that the particle has a finite size and moves due to the local average fluid velocity integrated over the particle volume. The particle angular velocity is determined from the vorticity in a similar manner, i.e.,

$$\Omega_i^n(t) = \frac{1}{2}\tilde{\omega}_i(t) = \int \frac{1}{2}\omega_i(\mathbf{x}, t) \Delta(\mathbf{x} - \mathbf{Y^n}, \sigma_\mathrm{d}) \, \mathrm{d}^3\mathbf{x}, \tag{14}$$

where Ω_i^n is the angular velocity of the nth particle and ω_i is the vorticity of the flow.

The two length scales σ_m and σ_d are found from solving two steady Stokes flow problems. Firstly, the length scale for the force monopole, σ_m, is determined by matching the settling velocity of a sphere falling in an infinite fluid with the Stokes settling velocity (Maxey and Patel, 2001). Secondly, the length scale for the force dipole, σ_d, is determined by matching the angular velocity of a steady sphere rotating in an infinite fluid with the Stokes angular velocity (Lomholt, 2000). These two matches result in

$$\frac{a}{\sigma_\mathrm{m}} = \sqrt{\pi} \approx 1.77 \quad \text{and} \quad \frac{a}{\sigma_\mathrm{d}} = \sqrt[3]{6\sqrt{\pi}} \approx 2.20. \tag{15}$$

More detailed descriptions of the method are given in Maxey and Patel (2001), Lomholt (2000), Lomholt and Maxey (2001) and Dent and Maxey (2000).

In the present work no lubrication or surface contact forces are included in the model. This was done deliberately in order to investigate the effects of the force coupling model without introducing any further models for lubrication or surface contact.

2.2. The numerical method

The force coupling Eqs. (1) and (2) have been solved numerically in a channel with periodic boundary conditions in the streamwise (x_1) and the spanwise (x_3) directions and no-slip boundary conditions in the normal direction (x_2). The computational geometry is shown in Fig. 1.

The equations are solved using a spectral method with Fourier expansions in the streamwise and the spanwise directions and Chebyshev polynomials in the normal direction. The original code was obtained from Handler et al. (1993). The program has been modified to include the force coupling terms and the particle tracking. In order to implement the iteration procedure for the force dipole strength, the time integration method was changed from a second order semi-implicit Adam–Bashforth/Crank–Nicolson method to a fully implicit second order Backward Difference Method (Schwarz, 1993). The iteration of the force dipole was continued until the components of $\tilde{E}_{ij}$ for all of the particles were below a certain value ϵ. Specifically the iteration ended when

$$\left\|\tilde{E}_{ij}\right\|^2 = \sum_i \sum_j \tilde{E}_{ij}^2 < \epsilon \quad \text{for } n = 1, \ldots, N, \| \tag{16}$$

or until a certain number of iterations is reached. The limit for the iteration was set to $\epsilon = 10^{-3}$ and the maximum number of iterations was set to 20. For the examples presented here the number of iterations were ranged from 6 for the low Reynolds number cases to 20 in the high Reynolds number cases. In the cases where the iterations did not converge to the desired level, the change in the force dipole strength, the particle velocity and the particle angular velocity between each step in the iteration was checked. The change in the force dipole strength was always lower than 0.5%, while the changes in the particle velocity and the particle angular velocity were less than 0.03%. Consequently, the effect of the lack of convergence to the level of $\|\tilde{E}_{ij}\|^2 < 10^{-3}$ on the results presented here is small. The fact that the iteration did not converge in the high Reynolds number case indicates that the procedure for determination of the force dipole given in Section 2.1 is best suited for low Reynolds number cases.

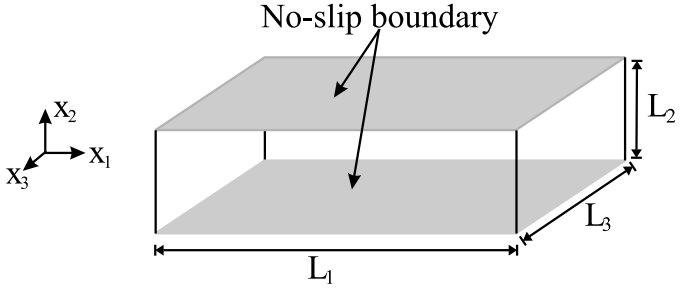

Fig. 1. Computational domain and coordinate system.

The particle trajectories are computed using an explicit third order Adam–Bashforth method. The explicit method made it possible to compute the new particle positions, before the solution to the flow field was determined. This choice was made in order to avoid computation of the particle positions in the iterations. Recomputing the particle positions would result in recomputing the envelope functions, which may be time consuming if many particles are present. A more complete description of the numerical scheme is given in Lomholt (2000).

The implicit scheme for time stepping allows relatively larger time steps to be used while still maintaining the accuracy of the computed flow as compared to a corresponding explicit scheme. In the results presented here, the CFL number for each direction of motion was continuously monitored during the course of a simulation and was kept below 0.5 with timesteps of the order $\delta t = 0.01$–0.1. This was most restrictive in the motion normal to the wall due to the nonuniform spacing of the grid points in this direction with the spectral scheme. Tests with smaller timesteps showed that there were no significant change in the computed particle velocities or particle trajectories. In the worst cases presented here (the three particle case and the high Reynolds number case in the inclined channel) reducing the timestep by a factor of 0.5 results in a change in the computed particle velocities of less than 10^{-4} and similarly for the particle trajectories.

3. Experimental setup

The numerical results of particle sedimentation presented in this paper will be compared with experiments. The setup for these experiments is shown in Fig. 2. The setup consists of a rectangular channel made in transparent PVC with height $L_1 = 150$ mm, width $L_2 = 10$ mm and depth $L_3 = 100$ mm. Thus, the aspect ratio of the channel is $L_3/L_2 = 10$. The numerical model described above is therefore a good approximation for particles moving in the center part (40 mm $< x_3 <$ 60 mm) of the channel. The fluid was a mixture of glycerol and water in order to achieve low Reynolds number conditions and larger viscosity than with pure water. The densities

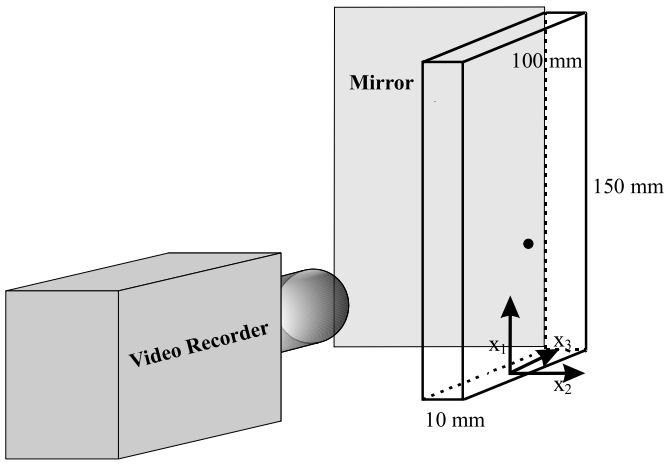

Fig. 2. Experimental setup.

of the mixtures used are shown in Table 1. The particles were polyamid spheres with a radius of $a = 1$ mm, thus the ratio of particle radius to channel width was $a/L_2 = 0.1$. The particles were introduced into the channel through five small holes in the bottom and since the density of the polymer particles was smaller than the fluid density, the particles moved upwards toward the top of the channel.

The motion of the particles was recorded by a standard CCD camera placed in front of the channel. Therefore the motion in the x_1x_2 plane is captured immediately. The motion in the x_1x_3 plane is captured using a mirror placed on the left-hand side of the channel at an angle of 45°. The single video camera captures the motion in both directions with 25 whole frames per second. The movie is saved either on video tape or directly to a hard disk. The particle trajectories are determined afterwards using the tracking software DigImage (Dalziel, 1992). The particle positions were determined as the weighted average of the intensities from the bright particle. In this way the positions were determined with an accuracy better than 0.1 mm. DigImage also computes the particle velocities from the time dependent trajectories. The error on the results for the particle position are ±0.1 mm and for the particle velocities it is ±0.1 mm/s.

The viscosity of glycerol solutions exhibit a strong sensitivity to temperature changes. Examples of the temperature dependence of various aqueous glycerol solutions are shown in Fig. 3, where the viscosity is shown as a function of the temperature. This shows that a temperature change of a few degrees may result in a relatively large change in the viscosity. Several techniques were tried to measure the viscosity directly, but this proved difficult due to the temperature sensitivity.

In the end the viscosity was determined by matching the computed velocity of a single particle with the experimentally measured velocity through a best fit procedure. The experiment at low Reynolds number with a single sphere satisfied the conditions for Stokes flow and so a comparison could be made with the analytical results given by Happel and Brenner (1965) for the streamwise velocity of the sphere moving in the center plane between two infinite walls. The viscosity determined by the matching procedure and by comparison with the analytical results agreed to within 2.5%.

Another problem is the tracking when two or more particles are present. Using the method described above, the particles are projected onto the x_1x_2 plane or the x_1x_3 plane. In these projections two particles will overlap, if the distance between their centers in one direction is smaller than the particle diameter. This overlap makes it impossible to track each particle by themselves,

Table 1
Experimental values[a]

Exp. no.	ρ_f (g/cm^3)	ρ_p (g/cm^3)	θ (°)	v (mm^2/s)	Re_p^{Stokes}
1	1.237	1.081	11.15	172.7	0.019
2	1.115	1.081	8.23	3.125	13.6
3 (•)	1.094	1.081	0.0	1.96	13.5
3 (▲)	1.094	1.081	0.0	1.96	13.5
4 (•)	1.179	1.081	0.0	15.31	1.55
4 (▲)	1.179	1.081	0.0	15.31	1.55
4 (▼)	1.179	1.075	0.0	15.31	1.64

[a] The symbols correspond to the symbols for the spheres shown in the figures.

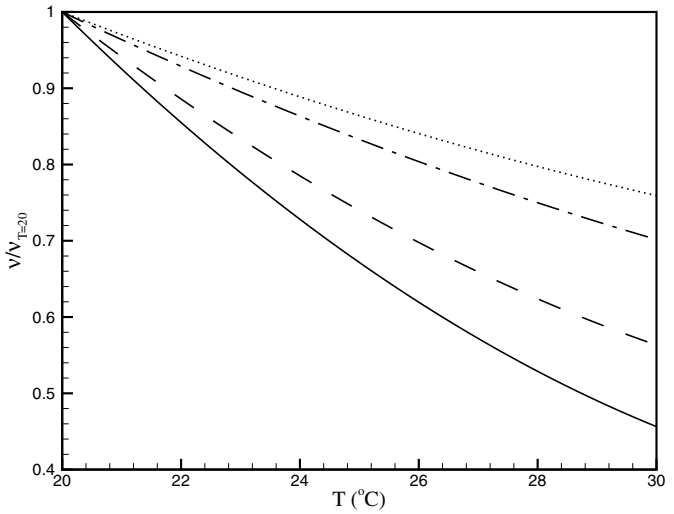

Fig. 3. Temperature dependency of various aqueous glycerol solutions. The viscosity has been normalized with the value at $T = 20$ °C. The data are from Kaye and Laby (1973). $(-)$ $\rho_f = 1.249$, $(- -)$ $\rho_f = 1.209$, $(- \cdot -)$ $\rho_f = 1.127$, and $(\cdots)$ $\rho_f = 1.061$.

because they become indistinguishable from each other. This causes the missing data values in experiments with more than one particle.

The experiments are characterized using a Reynolds number Re_p^{Stokes} based on the Stokes settling velocity W, i.e.,

$$Re_p^{Stokes} = \frac{2aW}{v} = \frac{2a}{v}\left|\frac{2a^2}{9\mu}(\rho_p - \rho_f)g\right| = \frac{4a^3}{9v^2}\left|\frac{\rho_p}{\rho_f} - 1\right|g, \tag{17}$$

where $g = 9.82\ \mathrm{m/s^2}$ is the absolute value of the gravitational acceleration.

4. Single sphere rising in inclined channel

The first two examples of particle motion are of a single sphere rising in an inclined channel. These examples serve two purposes;

- Is the force coupling method able to reproduce trajectories and velocities of a real particle?

Table 2
Computational parameters[a]

Exp. no.	$L_1 \times L_2 \times L_3$	$N_1 \times N_2 \times N_3$	δt	$Re = L_2U/v$	$Fr = gL_2/U^2$
1	$5 \times 1 \times 4$	$64 \times 32 \times 48$	0.1	0.579	982.0
2	$5 \times 1 \times 4$	$64 \times 32 \times 48$	0.01	32.0	982.0
3	$5 \times 1 \times 4$	$64 \times 32 \times 48$	0.01	51.0	982.0
4	$10 \times 1 \times 4$	$128 \times 32 \times 48$	0.01	6.53	982.0

[a] The characteristic length $L = L_2 = 10$ mm and the characteristic velocity $U = 10$ mm/s.

- Is the effect of the wall sufficiently represented?

The experiments were performed with the channel tilted an angle θ from the vertical (the top of the channel is moved to the left). The data for experiment numbers 1 and 2 are given in Table 1. Values of some of the important parameters used for the simulations are given in Table 2.

In Fig. 4 the results for $Re_p^{Stokes} = 0.019$ are presented. The particle trajectory is shown in subfigure (a), while the streamwise and the normal particle velocities are shown in subfigures (b) and (c), respectively. The positions and velocities are given in the frame of the experimental channel in mm and mm/s. The full drawn line shows the computational results with both the monopole and the dipole terms, while the dotted line denotes results from using the force monopole only. The experimental results are shown as (•). The straight upward line drawn at $x_2 = 4$ indicates the wall, i.e., when the center of the sphere is at $x_2 = 4$ the particle touches the wall. The straight line shown as dash-dot-dot in the figures corresponds to the direction of gravity in the frame of the channel. The error bars correspond to the errors of ± 0.1 mm for the positions and ± 0.1 mm/s for the velocities.

In the central part of the channel the agreement between the computed and the experimental trajectories is good, although the slope of the computed trajectories is slightly smaller than the slope of the experimental trajectory. Closer to the wall ($x_2 > 3$) the computed trajectories deviate from the experimental and the computational sphere moves through the wall ($x_2 > 4$). The reason

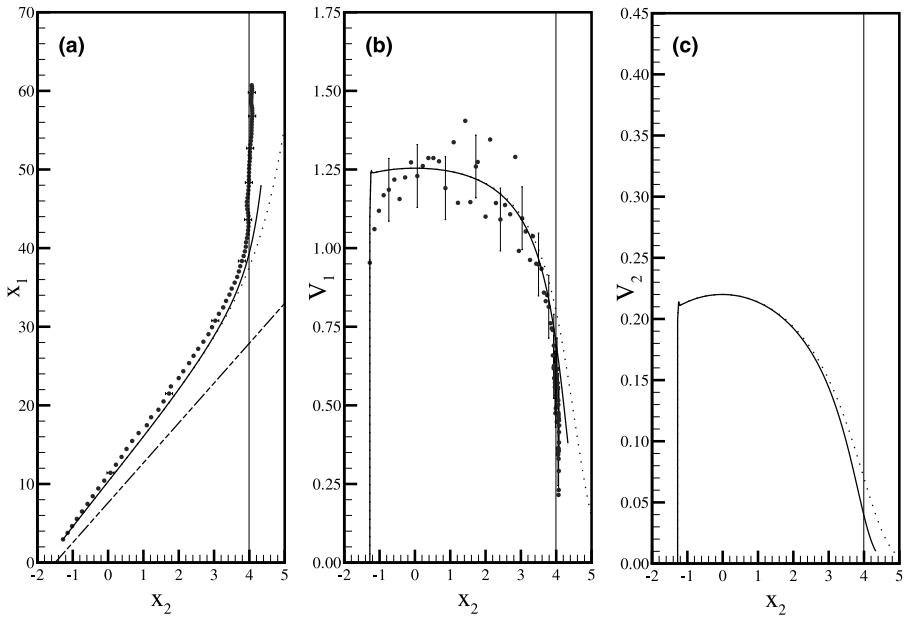

Fig. 4. Comparison of experimental and computed particle trajectory (a) and velocities ((b) upward and (c) lateral) in an inclined channel for $Re_p^{Stokes} = 0.019$. (•) Experiment, (–) FCM with both force terms, and (···) FCM with only the monopole. The line (– · ·–) indicate the direction of gravity in the frame of the channel. The error bars correspond to the errors of ± 0.1 mm for the positions and ± 0.1 mm/s for the velocities. The particle positions are given in mm and the velocities are in mm/s in the frame of the experimental setup.

for the underestimation of the wall effect is the lack of a fully resolved lubrication layer in the model and the absence of surface contact forces. When the sphere approaches the wall, a lubrication layer builds up between the sphere and the wall. During this build up the viscous dissipation slows down the sphere and ultimately the lateral motion of the sphere is stopped. This has also been found by Gondret et al. (1999). The reason it appears that the experimental sphere penetrates the wall is that the sphere is reflected on the wall and this moves the center of the sphere as seen by the camera, thus resulting in a measured position further to the left of the actual sphere position. In the force coupling simulation, the lubrication layer is only fully resolved if all the higher order multipoles are added to the force coupling terms (Kim and Karrila, 1991). Since only the force monopole and the force dipole are included, the sphere does not "feel" the full effect of the wall and continues through it. Neglecting the force dipole leads to a coarser representation of the flow field. Therefore the trajectory computed using only the force monopole deviates more from the experimental result than the trajectory computed using both force coupling terms. This becomes even more evident in the two figures for the particle velocities ((b) and (c) in Fig. 4). In these figures the difference between the two computed results becomes significant, when the sphere is about one radius away from the wall ($x_2 = 3$). A comparison between the computed velocities and the experimental velocities is more difficult, because of the scatter in the experimental data. The scatter is due to experimental uncertainties, since the velocities are small and therefore relatively difficult to measure. Nevertheless, the agreement is reasonably good for the streamwise velocity component. The experimental data for the normal velocity component are not shown because they were too small to be considered as measurable. The initial steep increase in the computed velocities, is due to the initial zero velocities of the computational spheres. Since we compute the particle velocity from the fluid velocity field, which results from the force the particle exerts on the fluid, it is not possible to specify an initial velocity of the particle. When the computational sphere is introduced, it will almost immediately attain the velocity of a freely sedimenting sphere. Therefore the curves in Figs. 4(b) and (c) initially appear as a step function, but they are continuous.

The second example is shown in Fig. 5. The Reynolds number for this case is $Re_p^{Stokes} = 13.6$. Again the computed trajectories and velocities agree well with those observed experimentally. In contrast to the above example, the difference between the two computations, with or without the force dipole term, is larger. The velocities from the two computations differ not only near the wall, but also in the middle of the channel, where the result from the force monopole shows a lower velocity than that from both force terms. The difference in the computed velocities is a result of the change in the rate of strain imposed by the force dipole. At small Reynolds numbers the rate of strain field is weak until the particle comes near the wall, but at larger Reynolds numbers the rate of strain field is significant also in the middle of the channel. Consequently, at this Reynolds number, the force dipole becomes important throughout the channel. This leads to a different velocity field in the region of the particle and therefore to a different particle velocity.

Fig. 5 shows that near the wall, there is no large deviation of the computed trajectories from the experimental trajectories. Hence, for the higher Reynolds numbers the force coupling method performs well all the way to the wall. An explanation could be that the viscous lubrication layer is much smaller when the Reynolds number increases. This explanation is supported by the findings of Gondret et al. (1999), they also observed that at finite Reynolds number the lubrication layer is thinner and its effect confined to a narrower region near the wall.

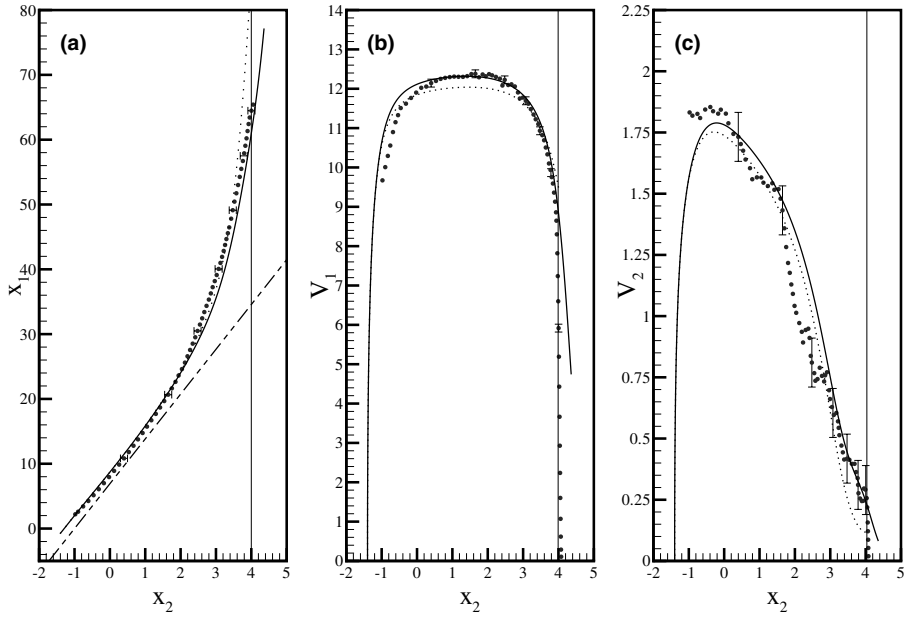

Fig. 5. Comparison of experimental and computed particle trajectory (a) and velocities ((b) upward and (c) lateral) in an inclined channel for $Re_p^{Stokes} = 13.6$. (•) Experiment, (–) FCM with both force terms, (· · ·) FCM with only the monopole. The line (– · –) indicate the direction of gravity in the frame of the channel. The error bars correspond to the errors of ±0.1 mm for the positions and ±0.1 mm/s for the velocities. The particle positions are given in mm and the velocities are in mm/s in the frame of the experimental setup.

5. Two spheres rising in a vertical channel

In this section an experiment with two equal spheres rising in a vertical channel will be compared with numerical results from the force coupling model. The aim of this experiment is:

- Is the force coupling method able to reproduce the drafting, kissing and tumbling procedure observed by Fortes et al. (1987) and Jayaweera et al. (1964)?

The data from the experiment are given in Table 1 and the parameters from the simulation are given in Table 2 for experiment 3.

The particle trajectories measured in the experiment are shown in Fig. 6. The symbol (▲) denotes the leading sphere and the symbol (•) denotes the trailing sphere. The first part of the figure ($x_1 < 73$) is the drafting period, where the trailing sphere moves faster than the leading sphere. As the trailing sphere approaches the leading sphere, it "pushes" the leading sphere aside. This is observed in both Figs. 6(a) and (b) for $60 < x_1 < 73$. The two spheres kiss at $x_1 \approx 73$. After the kiss, the trailing sphere tumbles around the leading sphere and they separate from each other. This result is consistent with the experiments of Jayaweera et al. (1964) and Fortes et al. (1987). For the sake of clarity no error bars are given on the figures for this case, but the errors of ±0.1 mm for the positions and ±0.1 mm/s for the velocities still applies.

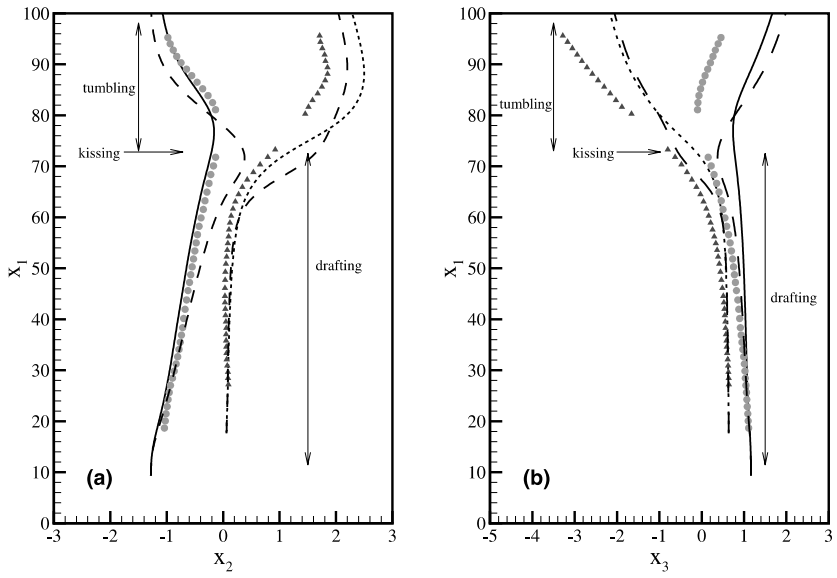

Fig. 6. Comparison of computed and experimental particle trajectories for two particles rising. Symbols denote the experiment and lines denote the computation. The dashed lines denotes computation with only the force monopole. The positions are given in mm in the frame of the experimental channel. The walls are at $x_2 = \pm 5$ mm. (a) streamwise–normal plane and (b) streamwise–spanwise plane.

The trajectories from the corresponding simulation with both force terms are shown as the full line and the dotted line in Fig. 6. The simulation agree qualitatively with the experiment. The discrepancy observed in Fig. 6(b) may result from a small error in the experimental values. In order to examine the reason for the discrepancy several experiments with a single sphere in the channel using the same liquid were performed. In these experiments the sphere was released in the middle of the channel and the trajectory of the single sphere was compared with a vertical string hanging beside the channel. The sphere in these experiments tended to drift either to the left or to the right. In a similar experiment at lower $Re_{\mathrm{p}}^{\mathrm{Stokes}}$ the drift was significantly reduced. The exact source for the drift at high Reynolds number is unknown. Some reasons could be a slowly re-circulating flow driven by temperature gradients or a disturbance flow created by the injection of the spheres through the small holes at the bottom. The difference between the simulation and the experiment seen in Fig. 6(a) results from the lack of lubrication forces and contact forces in the simulation. When the two spheres come close together these effects become important.

The effect of the force dipole on the trajectories is also shown in Fig. 6, where the trajectories computed using only the force monopole are shown as dashed lines. Results obtained with both force terms are better than those obtained with only the force monopole. Neglecting the force dipole, results in different trajectories not only in the kissing process, but also in the drafting and tumbling processes. Consequently, the force dipole is important throughout the DKT-process.

Fig. 7 shows a comparison of the particle velocities from the experiment with those from the simulation. The symbols denote the same spheres as in Fig. 6. The experimental data points around $t = 5.5$ s in the streamwise velocity are results from measurement errors due to a small part on the inner side of the front of the channel being dirty and should not be considered as part

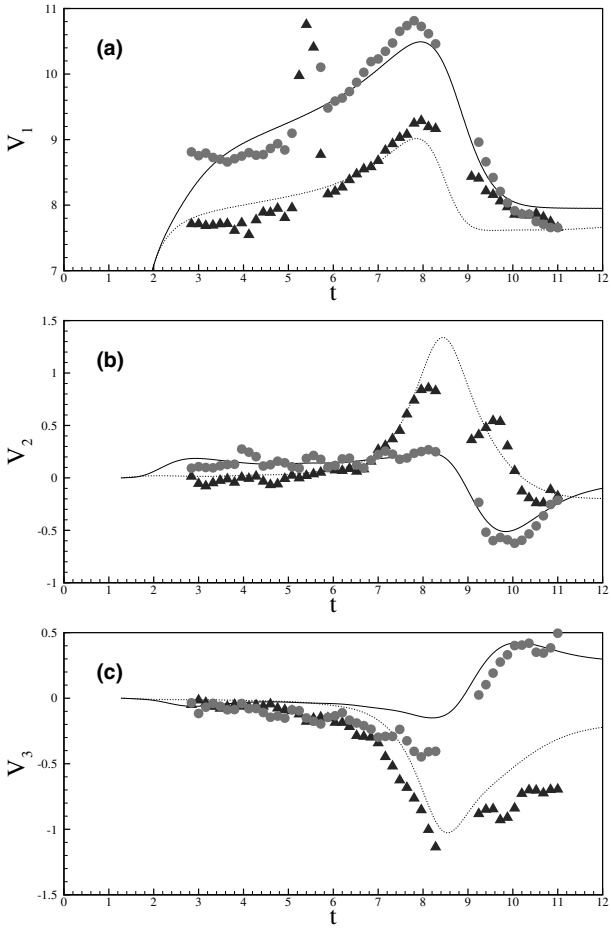

Fig. 7. Comparison of computed and experimental particle velocities for two particles rising. Symbols denote the experiment and lines denote the computation. The velocities are given in mm/s in the frame of the channel and time is in seconds: (a) streamwise velocity; (b) normal velocity and (c) spanwise velocity.

of the physical picture. The agreement in the figure is good, but two points should be noted. Firstly, the streamwise velocities in the simulation do not have the same maximum velocity as in the experiment. Furthermore, there is a larger difference in the computed streamwise velocities of the two spheres after the kiss. Therefore the trailing sphere overtakes the leading sphere. This is not the case in the experiment, where the two spheres settle on the same horizontal line and rise with equal streamwise velocity. Secondly, in the simulation the normal velocity of the leading sphere overshoots that observed experimentally. This is obviously related to the difference in the trajectories for the leading sphere seen in Fig. 6(a). The overshoot in the normal velocity and the difference in the streamwise velocities both results from the fact, that the interaction between the two spheres is not completely resolved.

In a previous investigation on two particle interaction using the force coupling method with just the force monopole, Maxey and Dent (1998) found that the particles were overlapping each other

before, during and after the kissing process. As in the present simulations no surface contact forces or lubrication layer effects were included in the simulations. In order to examine the overlap between the computational spheres in our example; the distance between the center of the spheres normalized with the diameter of the spheres is shown as function of time in Fig. 8. The horizontal line indicates where the distance between the sphere centers is equal to the diameter (the spheres touch each other). In the experiment the distance between the two spheres falls almost linearly with time until they kiss at $t \approx 8.5$ s. The initial separation after the kiss appears to increase linearly until $t \approx 10.5$ s, where the increase in the distance levels off. In the result obtained using only the force monopole, there is a considerable time of particle overlap. The two spheres overlap from $t = 7.8$ s to $t = 9.1$ s. On the other hand, in the result using both force terms, the two spheres do not actually kiss. Instead they begin to separate from each other, when the distance between their centers is about 1.3 times their diameter. Nevertheless, the distance from the result using both force terms is in better agreement with the experiments than from the result using only the force monopole. Based on this and the results for the single sphere, we may conclude that including the force dipole term yields the best results.

Vector plots of the velocity field at time $t = 7.88$ s are shown in Fig. 9. The velocity field is shown in the streamwise–normal plane at $x_3 = 0$ and in the streamwise–spanwise plane at $x_2 = 0$. The black circular areas are the cuts through the spheres in these planes. The difference in size is because the two spheres do not have the same x_3 and x_2 position. The flow around the leading sphere shows that the fluid is moving past the sphere. This faster moving fluid pushes the sphere aside, resulting in the increase in the normal and the spanwise velocities of the leading sphere seen in Fig. 7. On the other hand, the flow around the trailing sphere shows very little influence of the leading sphere. Therefore the trailing sphere moves in a more nearly straight line than the leading sphere, as observed in the trajectories in Fig. 6. However, due to the wake of the leading sphere, the trailing sphere moves into a fluid flow already moving in the same direction as the

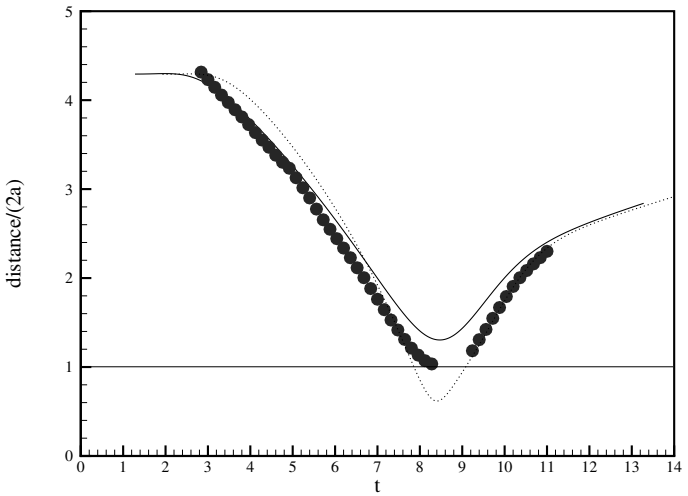

Fig. 8. Distance between the particles as function of time. (•) Experiment, (–) both force terms, and (· · ·) only the force monopole. Time is in seconds.

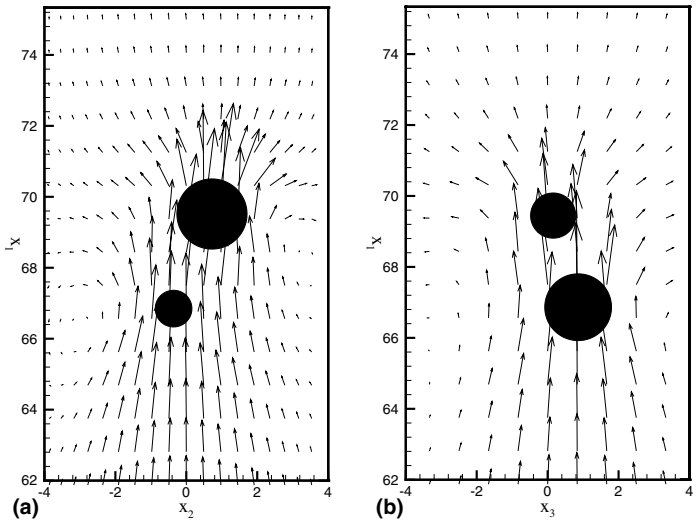

Fig. 9. Vector plot of the fluid velocity at time $t = 7.88$ s (before the spheres kiss). The vector plots are given in a plane with $x_3 = 0$ and a plane with $x_2 = 0$: (a) plane through $x_3 = 0$ and (b) plane through $x_2 = 0$.

sphere. Therefore the acceleration that the trailing sphere must provide to the surrounding fluid is diminished. This reduces the drag on the trailing sphere and it moves with a higher streamwise velocity than the leading sphere, as observed in Fig. 7.

The velocity field after the kiss at time $t = 9.08$ s is given in Fig. 10. The velocity field in the streamwise–normal plane at $x_2 = 0$ is shown in Fig. 10(a) and the velocity field in the streamwise–

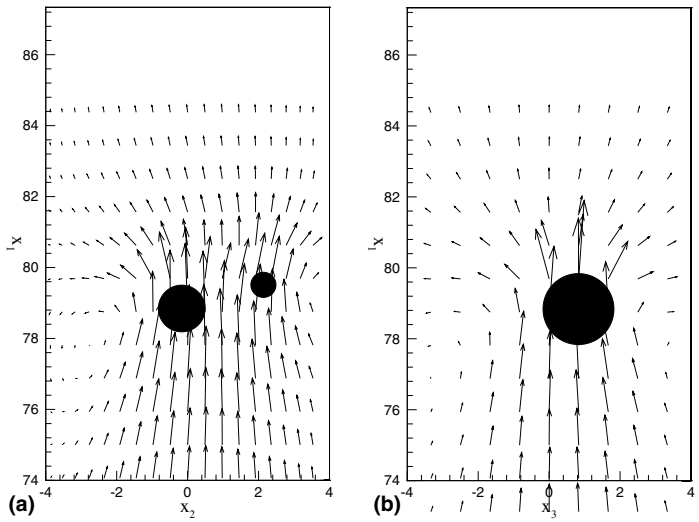

Fig. 10. Vector plot of the fluid velocity at time $t = 9.08$ s (after the spheres kiss). The vector plots are given in a plane with $x_3 = 0$ and a plane with $x_2 = -0.183$ (center of trailing sphere): (a) plane through $x_3 = 0$ and (b) plane through $x_2 = -0.183$ (center of trailing sphere).

spanwise plane through the center of the trailing sphere ($x_2 = -0.183$) is shown in Fig. 10(b). At this time the flow around the trailing sphere has changed considerably. First consider Fig. 10(a). Due to the presence of the leading sphere, the flow to the right of the trailing sphere is stronger than the flow to the left. This makes the trailing sphere move to the left as observed in the trajectory in Fig. 6(a) and the normal velocity in Fig. 7(b). In Fig. 10(b) the flow is stronger on the left-side of the sphere, forcing the sphere to the right as seen in Fig. 6(b). These changes in the fluid flow indicates that, the pushing effect changes direction, when the trailing sphere has reached the leading sphere. Before the kiss, the trailing sphere was pushing the leading sphere, but after the kiss the leading sphere begins to push on the trailing sphere. The change is probably due to several effects. Firstly, the trailing spheres move faster than the leading sphere and therefore it will overtake the leading sphere. In order to do so, the trailing sphere must either push the leading sphere aside or go around it. The velocity fields indicate that the trailing sphere does both. Secondly, at the time of the kiss the trailing sphere is closer to the middle of the channel than the leading sphere. Therefore the lift force from the walls is smaller on the trailing sphere than on the leading sphere. Hence, it may be "easier" for the trailing sphere to go around the leading sphere instead of trying to push it aside.

In the tumbling process the two spheres roll around each other. This is illustrated in Fig. 11, where the computed angular velocities of the two spheres from the simulation are given as a function of time. Also given is the distance between the spheres. From this figure it is clear that as the trailing sphere approaches the leading sphere, the rotation of the spheres increases and in the tumbling process the trailing sphere rolls around the leading sphere. The rotation about the x_2-axis of the trailing sphere prior to the kiss, is due to the wake of the leading sphere. Similarly for the rotation about the x_3-axis, but for this direction the presence of the walls also causes the sphere

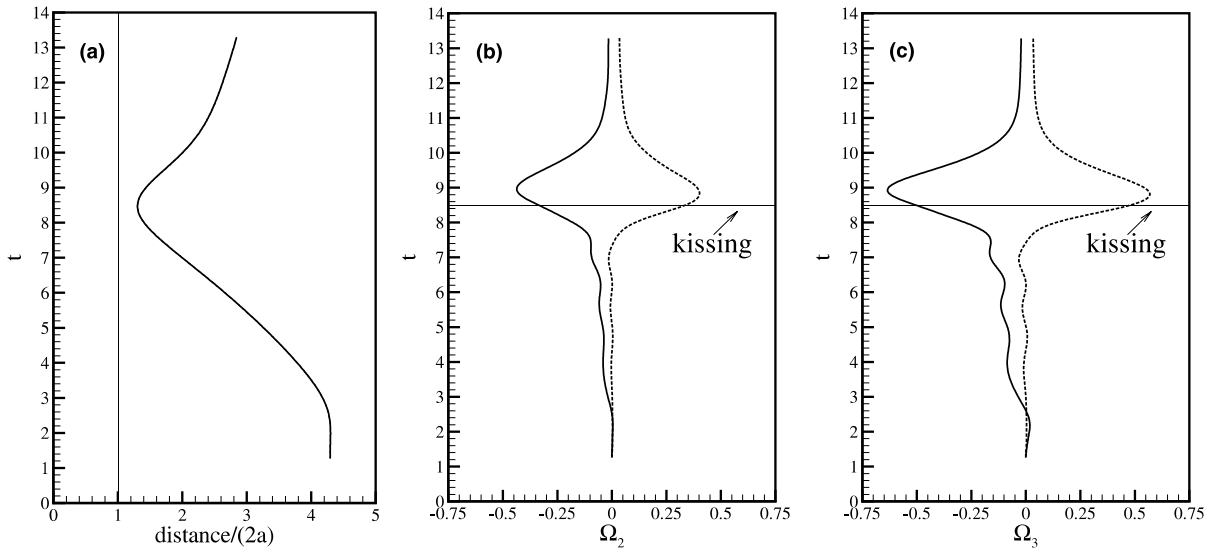

Fig. 11. Angular velocity as function of time for the particles in the simulation. The angular velocities are given in s^{-1} and time is in seconds: (a) distance between the spheres; (b) rotation about x_2-axis; and (c) rotation about x_3-axis.

to rotate. This may be the reason for the higher angular velocity about the x_3-axis than about the x_2-axis. The final rotation of the spheres agrees with the findings of Jayaweera et al. (1964). In their experiments on two sphere interaction at low Reynolds numbers, they observed that after the kiss the two spheres separate and rotate in opposite directions. However, Jayaweera et al. (1964) did not observe any rotation before the two spheres kiss. A reason could be that they performed their experiments in a large tank, not in a channel, therefore there was no wall effect on the spheres. Another possibility is the low value of the Reynolds number in their experiments, which may limit the rotation of the trailing sphere. Supporting this speculation is another simulation by Lomholt (2000) of two interacting spheres at $Re_p = 1.55$, where the trailing sphere also rotates before the spheres kiss. The rate of rotation is diminished indicating that decreasing the Reynolds number results in a decrease of the rotation rate before the kiss.

6. Three spheres rising in a vertical channel

The final example of particles rising in a channel is with three spheres. The experimental data for experiment 4 are given in Table 1. Although it was attempted to have three equal spheres, sphere (▼) had a density slightly lower than the other two particles. The computational parameters are given in Table 2.

The trajectories from the experiment are drawn in Fig. 12. The symbols in the figure correspond to the symbols in Table 1. Initially the sphere (▲) is the leading sphere, the sphere (●) is the middle

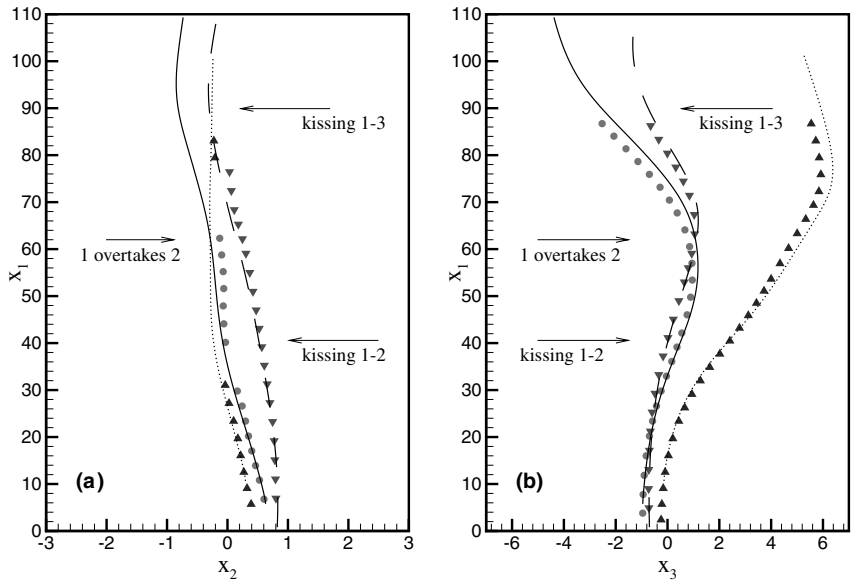

Fig. 12. Comparison of computed and experimental particle trajectories for three particles rising. Symbols denote the experiment and lines denote the computation. The positions are given in mm in the frame of the experimental channel. The walls are at $x_2 = \pm 5$ mm: (a) streamwise–normal plane and (b) streamwise–spanwise plane.

sphere and the sphere (▼) is the trailing sphere. During the experiment two kissing events appear. The first is at $t = 5.2$ s between spheres (▲) and (•), this is denoted as *kissing 1–2* in Fig. 12. The second event appears at $t = 9.6$ s just after the spheres leave the view of the camera. The time and place for this event is determined from the simulation. This second kissing event is between spheres (•) and (▼) and is denoted as *kissing 1–3* in Fig. 12. These two kissing events correspond to two drafting and tumbling processes as shown below. Furthermore, the sphere initially leading (sphere (▲)) is overtaken by the other two spheres. The position, where sphere (•) overtakes sphere (▲) is denoted as *1 overtakes 2* in Fig. 12. For the sake of clarity no error bars are given on the figures for this case, but the errors of ± 0.1 mm for the positions and ± 0.1 mm/s for the velocities still applies.

The trajectories from the simulation are shown as the lines in Fig. 12. The full drawn line corresponds to sphere (•), the dotted line corresponds to sphere (▲) and the dashed line corresponds to sphere (▼). The agreement between the experiment and the simulation is good. The computation has been continued beyond the experiment in order to capture the second kissing event and to show that the sphere initially leading (sphere (▲)) is left behind by the other two spheres. This is best seen in Fig. 12(b). The final streamwise position of sphere (▲) is approximately 100 mm, while the final streamwise position of spheres (•) and (▼) are approximately 110 mm. The interaction between the spheres in the two DKT-processes, causes the sphere (▲) to be left behind. In the first DKT-process the leading sphere is pushed aside by the middle sphere and it moves away from the two trailing spheres in the spanwise direction. Due to the DKT-process between sphere (•) and sphere (▼), these two spheres begin to move as a particle pair. This leads to a higher streamwise velocity of the two trailing spheres than of the leading sphere. Therefore the two trailing spheres overtake the leading sphere, leaving it behind.

The particle velocities from both experiment and simulation are shown in Fig. 13. The symbols and the lines denote the same particles as in Fig. 12. In the first part of the figure for $t = 1$ s to $t = 6.5$ s, the streamwise velocities for the leading sphere (▲) and the middle sphere (•) are similar to the velocities observed in Fig. 13(a) for the two particle examples. This part of the figure corresponds to the first DKT-process. The similarity of the velocities indicate that the DKT-process between the sphere (▲) and sphere (•) is independent of the trailing sphere (▼). During the DKT-process of the two leading spheres, the distance between sphere (•) and sphere (▼) increases. Therefore the drafting of sphere (▼) in the wake of sphere (•) is diminished, leading to the decrease in the streamwise velocity of sphere (▼). In the kissing and tumbling process between sphere (▲) and sphere (•) the streamwise velocity of these two spheres decreases. At time $t = 5.5$ s this results in the streamwise velocity of sphere (▼) being the highest. Thus, the distance between sphere (•) and sphere (▼) decreases and a drafting process between these two spheres is initiated. At time $t = 7.2$ s the sphere (▼) is within one diameter of the sphere (•). Due to the higher velocity of sphere (▼) it begins to push fluid around sphere (•), thereby starting a pushing of sphere (•) as described above for the two particle examples. This leads to the increase in the streamwise velocity of sphere (•) seen in Fig. 13(a) for $t = 7.2$ s to $t = 8.2$ s. The drafting of sphere (▼) initiated at $t = 5.5$ s ends at $t = 9.6$ s, where the kissing event between sphere (•) and sphere (▼) appears. The form of the curves for the streamwise velocity of spheres (•) and (▼) during their DKT-process from $t = 7.2$ s to $t = 11.5$ s, is reminiscent of the streamwise velocity observed in the DKT-processes of dual particles shown in Figs. 13(a). This indicates that sphere (▲) has little effect on the

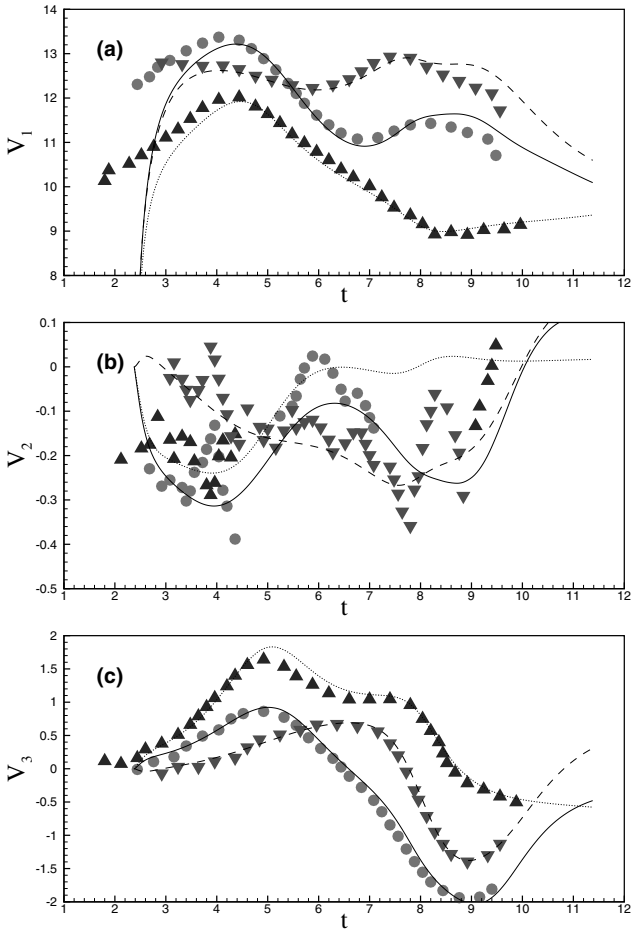

Fig. 13. Comparison of computed and experimental particle velocities for three particles rising. Symbols denote the experiment and lines denote the computation. The velocities are given in mm/s in the frame of the channel and time is in seconds: (a) streamwise velocity; (b) normal velocity, and (c) spanwise velocity.

interaction between the other two spheres. The fact that one sphere is left behind agrees with the findings of Jayaweera et al. (1964).

7. Conclusion

A force coupling method for computing particulate flows with rigid spheres has been described. Numerical results from the method were compared with experiments on one, two and three spheres in a channel. The verification of the method shows that it gives good results for Reynolds numbers up to approximately 15 based on the Stokes settling velocity and the sphere diameter.

The strengths of the method are the relatively fast computation and the possibility to implement it in any existing code for the solution of the Navier–Stokes equations.

Acknowledgements

The authors would like to thank R. Handler for providing the original channel code used for the simulation presented in this paper. S. Lomholt would like to thank Risø National Laboratory and UNI•C the Danish Computing Centre for Research and Education for their financial support. M. Maxey wishes to acknowledge support from the National Science Foundation, award CTS 9424169 and the National Center for Microgravity Research, Independent Studies Program (award USRA 4500-03).

References

Dalziel, S.B., 1992. Decay of rotating turbulence: some particle tracing experiments. Appl. Scientific Res. 49, 217–244.

Dent, G.L., 1999. Aspects of Particle Sedimentation in Dilute Flows at Finite Reynolds Numbers. Ph.D. Thesis, Brown University, Providence, RI.

Dent, G.L., Maxey, M.R. 2000. Flow through a periodic array of particles at finite Reynolds numbers. Phys. Fluids, submitted.

Esmaeeli, A., Tryggvason, G., 1998. Direct numerical simulations of bubbly flows. Part 1. Low Reynolds number arrays. J. Fluid Mech. 377, 313–345.

Feng, J., Hu, H.H., Joseph, D.D., 1994. Direct numerical simulation of initial value problems for the motion of solid bodies in a Newtonian fluid. Part 1. Sedimentation. J. Fluid Mech. 261, 95–134.

Fortes, A.F., Joseph, D.D., Lundgren, T.S., 1987. Nonlinear mechanics of fluidization of beds of spherical particles. J. Fluid Mech. 177, 467–483.

Glowinski, R., Pan, T.W., Hesla, T.I., Joseph, D.D., 1999. A distributed Lagrange multiplier/fictitious domain method for particulate flows. Int. J. Multiphase Flow 25, 755–794.

Gondret, P., Hallouin, E., Lance, M., Petit, L., 1999. Experiments on the motion of a solid sphere toward a wall: From viscous dissipation to elastohydrodynamic bouncing. Phys. Fluids 11, 2803–2805.

Handler, R., Levich, E., Sirovich, L., 1993. Drag reduction in turbulent channel flow by phase randomization. Phys. Fluids A 5 (3), 686–694.

Happel, J., Brenner, H., 1965. Low Reynolds Number Hydrodynamics. Prentice-Hall, Englewood Cliffs, NJ.

Hu, H.H., 1996. Direct simulation of flows of solid–liquid mixtures. Int. J. Multiphase Flow 22, 335–352.

Jayaweera, K.O.L.F., Mason, B.J., Slack, G.W., 1964. The behaviour of clusters of spheres falling in a viscous fluid. Part 1. Experiment. J. Fluid Mech. 20 (19), 121–128.

Johnson, A.A., Tezduyar, T.E., 1997. 3D simulation of fluid–particle interactions with the number of particles reaching 100. Comput. Meth. Appl. Mech. Eng. 145, 301–321.

Kaye, G.W.C., Laby, T.H., 1973. Tables of Physical and Chemical Constants, 14th ed. Longman, New York.

Kim, I., Elghobashi, S., Sirignano, W.A., 1998. On the equation of motion for spherical-particle motion: Effect of Reynolds and acceleration numbers. J. Fluid Mech. 367, 221–253.

Kim, S., Karrila, S.J., 1991. Microhydrodynamics: Principles and Selected Applications. Butterworth-Heinemann, London.

Lawrence, C.J., Mei, R., 1995. Long-time behaviour of the drag on a body in impulsive motion. J. Fluid Mech. 283, 307–327.

Lomholt, S., 2000. Numerical investigations of macroscopic particle dynamics in microflows. Ph.D. Thesis. Risø National Laboratory, Roskilde, Denmark.

Lomholt, S., Maxey, M.R., 2001. Force coupling method for particles sedimenting in a channel: Stokes flow. J. Comp. Phys., submitted.

Maxey, M.R., Riley, J.J., 1983. Equation of motion for a small rigid sphere in a nonuniform flow. Phys. Fluids 26, 883–889.

Maxey, M.R., Patel, B.K., Chang, E.J., Wang, L.-P., 1997. Simulations of dispersed turbulent multiphase flow. Fluid Dyn. Res. 20, 143–156.

Maxey, M.R., Dent, G.L., 1998. Some features of particle sedimentation at finite Reynolds numbers. In: Third International Conference Multiphase Flow ICMF98, June 8–12, Lyon, France.

Maxey, M.R., Patel, B.K., 2001. Localized force representations for particles sedimenting in Stokes flow. Int. J. Multiphase Flow 27, 1603–1626.

Michaelides, E.E., 1997. Review – the transient equation of motion for particles, bubbles, and droplets. J. Fluids Eng. 119, 233–247.

Schwarz, H.R., 1993. Numerische Mathematik. B.G. Teubner, Stuttgart.

Wu, J., Manasseh, R., 1998. Dynamics of dual-particles settling under gravity. Int. J. Multiphase Flow 24, 1343–1358.